Bioorganic Chemistry 89 (2019) 103033

Contents lists available at ScienceDirect

Bioorganic Chemistry

journal homepage: www.elsevier.com/locate/bioorg

N-aryl-*N*'-ureido-*O*-sulfamates: Potent and selective inhibitors of the human Carbonic Anhydrase VII isoform with neuropathic pain relieving properties

Murat Bozdag[a,1], Giulio Poli[b,1], Andrea Angeli[a], Elena Lucarini[c], Tiziano Tuccinardi[b], Lorenzo Di Cesare Mannelli[c], Silvia Selleri[a], Carla Ghelardini[c], Jean-Yves Winum[d], Fabrizio Carta[a,*], Claudiu T. Supuran[a,*]

[a] University of Florence, NEUROFARBA Dept., Sezione di Scienze Farmaceutiche e Nutraceutiche, Via Ugo Schiff 6, 50019 Sesto Fiorentino, Florence, Italy
[b] University of Pisa, Department of Pharmacy, Via Bonanno 6, 56126 Pisa, Italy
[c] University of Florence, NEUROFARBA Dept., Sezione di Farmacologia e Tossicologia, Viale Gaetano Pieraccini 6, 50139 Florence, Italy
[d] Institut des Biomolécules Max Mousseron (IBMM), UMR 5247 CNRS, ENSCM, Université de Montpellier, 240 avenue du Professeur Emile Jeanbrau, 34296 Montpellier Cedex 05, France

ARTICLE INFO

Keywords:
Carbonic Anhydrase
Neuropathic pain
Carbonic Anhydrase Inhibitors
N-aryl-*N*'-ureido-*O*-sulfamates

ABSTRACT

Herein we report for the first time an efficient synthetic procedure for the preparation of *N*-aryl-*N*'-ureido-*O*-sulfamates (**AUSs**) as a new class of Carbonic Anhydrase Inhibitors (CAIs). The compounds were tested for the inhibition of several human (h) Carbonic Anhydrase (CA; EC 4.2.1.1) isoforms. Interesting inhibition activity and high selectivity against CA VII and XII versus CA I and II, with K_Is in the low nanomolar range, were observed. Molecular modeling studies allowed us to decipher the structural features underpinning the selective inhibitory profile of AUSs towards isoforms CAs VII and XII. A selection of sulfamates showed promising neuropathic pain modulating effects in an in vivo animal model of oxaliplatin induced pain.

1. Introduction

The last decade has been characterized by a particularly sustained research in the field of pain, which culminated in 2011 with a new definition of neuropathic pain [1]. A task force of experts called the Special Interest Group on Neuropathic Pain (NeuPSIG) within the International Association for the Study of Pain (IASP) firstly suggested, by means of a consensus paper, that neuropathic pain should be properly defined as "*arising as a direct consequence of a lesion or disease affecting the somatosensory system*" [1,2]. This new definition, which was almost acquired from IASP, differs from the previous one for the missing word "*dysfunction*". What apparently did look like a mere debate on descriptions, it was the necessary step to elude serious and stringent limitations imposed from the previous definition in the diagnosis, classification, epidemiology, treatment and thus in research and development within the neuropathic pain field. In this context are also our efforts on structure-based drug design studies towards the validation of Carbonic Anhydrase (CA; EC 4.2.1.1) enzymes for the management of neuropathic pain. This is also in agreement with the intent of the NeuPSIG committee to raise scientific awareness as well as to define a new scientific playground in the field.

The link between CAs and neuropathic pain was first raised by Kaila and Price by reporting that the CAs catalyzed reaction had significant effects on the regulation of the levels of several neurotransmitters, among which γ-aminobutyric acid (GABA) [3,4]. These first experiments were based on the administration of the non-selective CA inhibitors (CAIs) (e.g. acetazolamide-**AAZ**), but they clearly showed an effect when the drug was administered in combination with midazolam [5–7]. Current knowledge however lacks any evidence on which CA isoforms, among the 15 catalytically active expressed ones in humans, are mainly involved in peripheral and/or central sensitization events leading to neuropathic pain. Furthermore, the precise mechanism of action of CAIs in modulating neuropathic pain seems to be rather complex, as both the levels of GABA as well as the activity of the K-Cl cotransporter KCC2 are affected by inhibiting the enzyme at the central and probably peripheral levels.

Therefore, we turned our attention towards the physiologically relevant hCAs present in the nervous system, i.e., isoforms I, II, VII, IX and XII, which are largely expressed both at the central as well as at peripheral level. Among them, the CA VII is mainly present within the

* Corresponding authors.
E-mail addresses: fabrizio.carta@unifi.it (F. Carta), claudiu.supuran@unifi.it (C.T. Supuran).
[1] These Authors contributed equally.

https://doi.org/10.1016/j.bioorg.2019.103033
Received 6 April 2019; Received in revised form 20 May 2019; Accepted 3 June 2019
Available online 06 June 2019

central nervous system (CNS) and this makes it particularly interesting when designing selective CAIs for neuropathic pain management purposes.

The concept of isoform selectivity is of paramount importance within the CAs field, as the various enzymatic isoforms are highly specialized in catalyzing the CO_2 hydration reaction and they all differ for expression within specific cellular and tissutal districts [8]. Our efforts in pursuing this goal by means of structure-based drug discovery led to the identification of new chemical classes acting as CAIs such as the coumarins [9,10] and their congeners [11–16], the phenols [17], the polyamines [18], the dithiocarbamates [19,20] and their bioisosteres [21,22], the 2-benzylsulfinylbenzoic acids [23], the benzoxaboroles [24] and the last introduced the selenols [25]. All of them were demonstrated to possess diverse inhibition mechanisms by means of inhibition experiments as well as X-ray crystallographic investigations of the corresponding adducts within various hCAs [8–19]. A neglected moiety reported by some of us is the low micromolar CAI inhibitors *N*-hydroxyurea, which was demonstrated to interact as a bidentate zinc-binding group within the hCA II enzymatic cleft [26]. With our surprise no further developments of *N*-hydroxy urea-based CAIs were carried out since their first report in 2006, also in consideration of the reappraisal of the ureido moiety by means of our investigations [27–29], which led to the introduction in clinical phase II of the small molecule **SLC-0111** (Fig. 1), in association with gemcitabine, for the treatment of metastatic pancreatic ductal cancer [30].

In the present study we propose the *N*-aryl-*N'*-ureido-*O*-sulfamates (**AUSs**) as a new class of CA ligands, which was conceived by merging the chemical groups proven to be particularly relevant within the CAI field, as schematically represented in Fig. 1, and thus virtually encompassing their properties.

As part of this study, we developed an efficient synthetic method to afford *N*-aryl-*N'*-ureido-*O*-sulfamates in good yields. Thus, the series obtained was investigated for the ability to inhibit the human expressed CAs, followed by investigation of the binding modes by means of molecular modelling studies. In consideration of the excellent selectivity of the compounds reported for the hCA VII, we investigated their effects in an in vivo model of neuropathic pain (see Fig. 2.).

2. Results and discussion

2.1. Design and synthesis of compounds

The strategic approach beneath our research studies relies on the recently reported coordination properties of the hydroxylamine-*O*-

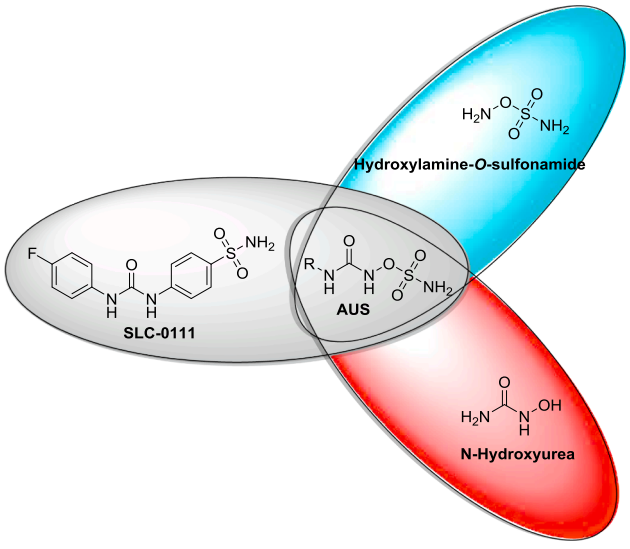

Fig. 1. Schematical representation of the design approach used in this study.

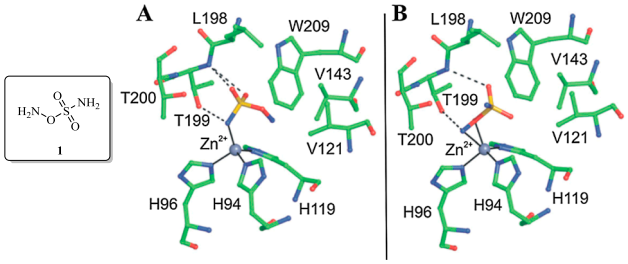

Fig. 2. Zn (II) coordination geometry in the hCA II/**1** adduct for binding according to a tetrahedral (**A**) or penta-coordinated (**B**) cluster. Hydrogen bonds and residues forming van der Waals interactions are also reported [31].

sulfonamide **1** compound towards various hCAs [31].

As shown above, two Zn (II) coordination patterns were reported: (*i*) direct coordination of the inhibitor to the metal ion to form a tetrahedral adduct, in agreement to the coordination cluster of CAIs of the sulfonamide type and their bioisosteres [32]; (*ii*) generation of a penta-coordinated metal ion based complex in which the aminooxy moiety in **1** interacts in a side-on (η^2) manner [32]. Such a discovery defined **1** as a blueprint for further development of CAIs bearing the sulfonamides or aminoxysulfamates as zinc binding moieties. In this context, we designed and developed a synthetic strategy with the aim to obtain CAIs bearing the hydroxylamine-*O*-sulfonamide moiety with a coordination pattern entirely shifted to the type reported in Fig. 2**A**. According to our expectations, compounds of this type will benefit of the strong interaction of the sulfamate moiety to the Zn (II) ion as well as of the flexibility features the ureido group may retain, which proved to be vital for directing the inhibition preferentially towards physiologically relevant hCAs [27,28,33]. Our first synthetic attempt was based on the previously reported methodology to obtain the hydroxylamine-*O*-sulfonamide **1a** as the trifluoroacetic acid salt, which in turn was reacted with commercially available isocyanates as reported in Scheme 1.

Although the synthetic procedure proved successful, the purification of the final compounds, by means of flash chromatography or crystallization techniques, resulted quite inefficient as significative decomposition occurred. Alternatively, the final compounds were recovered in good yields by treatment of the corresponding hydroxyureas **2a-22a** [33] with calculated excess of freshly prepared sulfamoyl chloride at 0 °C in anhydrous DMA. Usually the starting materials were consumed in 5–10 min (TLC monitoring) and the reactions were quenched with slush followed by acidification with a 1.0 M HCl aqueous solution. The desired compounds **2–22** were isolated in good yields according to the treatments described in the experimental section with a HPLC purity grade of ≥ 95% (see Scheme 2.).

2.2. Carbonic Anhydrase inhibition

The reported compounds **2–22** were tested *in vitro* for their inhibitory properties against the physiologically relevant hCA isoforms (e.g. I, II, VII, IX, XII) by means of the stopped-flow carbon dioxide assay [34] and compared with the clinically used drug Acetazolamide (**AAZ**) (Table 1).

The following structure-activity relationships (SARs) can be drawn:

i) The majority of compounds tested were weak inhibitors of the kinetically slowest hCA I isoform with K_I values spanning between 347.6 and 8921.0 nM, whereas the remaining ones were ineffective (K_Is > 10000). The most potent inhibitor was **12** (K_I of 347.6 nM) which possessed the ethoxy group at 2 position of the phenyl ring, followed by the indene containing scaffold **21** (K_I of 863.3 nM) and **13** (K_I of 902.4 nM) which contained the bulky 4-phenoxy moiety. The results reported in Table 1 didn't allow to define a clear SAR for this isoform.

ii) The abundantly expressed cytosolic isoform hCA II, in analogy to

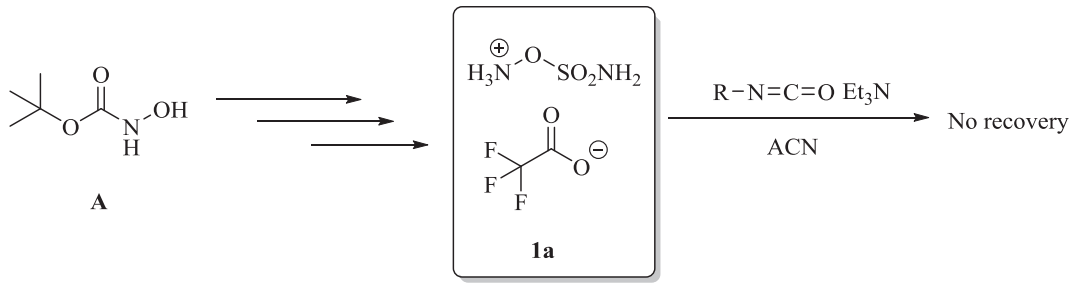

Scheme 1. General synthetic scheme for *N*-aryl-*N'*-ureido-*O*-sulfamates.

previous one, was poorly inhibited by the series of sulfamates **2–22**. The most efficient inhibitor of the series was **18** (K_I of 295.5 nM) that possessed the 4-fluoro-3-methyl substitution pattern, followed by the unsubstituted derivative **2** and 4-trifluoromethyl substituted derivative **17** (K_Is of 620.2 and 645.6 nM, respectively). All the remaining compounds resulted weak inhibitors with K_Is between 1.72 and 7.28 μM).

iii) Compounds **2–22** were effective inhibitors of the CNS abundantly expressed hCA VII isoform. As reported in Table 1, all the K_I values were comprised in the nanomolar concentration range, spanning between 2.1 and 57.4 nM, and were thus comparable to the standard CAI **AAZ** (K_I of 6.0 nM). Among the series tested, compounds **2**, **4–11**, **15–19** showed low nanomolar inhibitory activities with K_Is between 2.1 and 8.1 nM. The most potent one was the 3-chlorophenyl derivative **6** which was 2.86-fold more potent when compared to **AAZ** (K_Is of 2.1 and 6.0 nM, respectively). Slightly higher K_I values were obtained for compounds **16** (3,5-dimethyl substituted), **8** (4-fluoro substituted) and **2** (unsubstituted) with K_Is in the range of 2.3–2.8 nM. Even the remaining compounds in the series (e.g. **3**, **12–14**, **20–22**) were effective inhibitors of this isoform and reported K_I values spanning between 19.6 and 57.8 nM.

iv) The tumor associated transmembrane isoform hCA IX was inhibited only by 12 compounds out of the 21 tested, and among them the 3-ethylester phenyl substituted **14** and the indan-5-yl derivative **21** were the most potent (K_Is of 15.5 and 11.5 nM, respectively) also when compared to **AAZ** (K_I of 25.8). The remaining compounds were medium potency inhibitors (e.g. **6, 10** and **22**) with K_Is of 193.1, 244.2 and 266.6 nM respectively. As for the remaining ones (e.g. **2, 13** and **16**) low micromolar K_I values were obtained and comprised between 3.05 and 3.76.

v) The second tumor associated isoform, the hCA XII, was effectively inhibited by the compounds reported here with low nanomolar inhibitory constants. This isoform was highly inhibited by the 2-nitro- and 4-chloro-phenyl substituted derivatives **10** and **5**, with K_Is of 6.1 and 7.5 nM, respectively, that are comparable to **AAZ** (K_I of 5.7 nM). As for the remaining ones, three main blocks may be defined. The first is represented by compounds **2, 8, 15** and **16**, which do possess K_I values comprised between 18.9 and 26.1 nM; the second block comprises derivatives **3, 4, 11, 17** and **19** (K_Is between 33.2 and 52.2 nM); the latter includes the remaining compounds tested, which exhibited higher nanomolar kinetic values.

The series of *N*-phenyl-*N'*-ureido-*O*-sulfamates were assayed on all physiologically relevant hCAs. In the whole, the compounds here reported were high potent inhibitors of the CNS expressed hCA VII isoform, with low nanomolar inhibition values comparable to the standard CAI **AAZ**. Only few compounds (e.g. **12–14** and **22**) showed K_I values in the medium-high nanomolar range. The compounds tested showed also good inhibition of the tumor associated hCA XII, with K_I values below

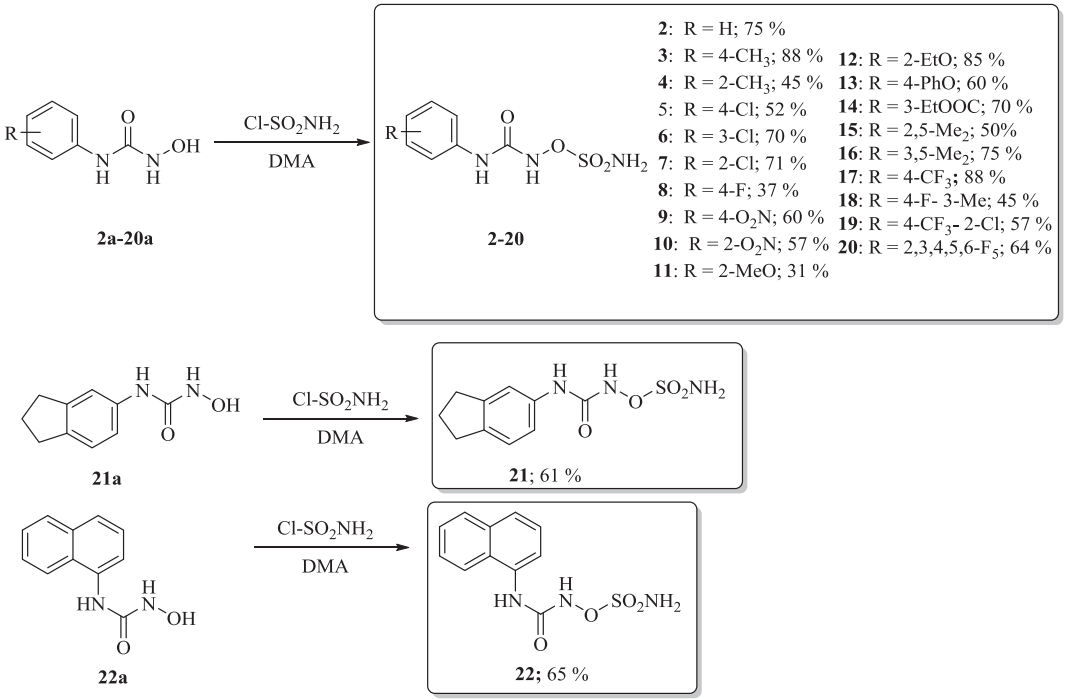

Scheme 2. Synthesis of *N*-aryl-*N'*-ureido-*O*-sulfamates **2–22.** Percentage yields are reported.

Table 1
Stopped-flow kinetic data of compounds **2–22** on hCAs I, II, VII, IX and XII in comparison with **AAZ**.

	K_I (nM)*				
Compound	hCAI	hCAII	hCAVII	hCAIX	hCAXII
2	7894.9	620.2	2.8	3051.9	26.1
3	> 10000	4178.0	26.0	> 10000	37.9
4	> 10000	2016.6	4.6	> 10000	52.2
5	> 10000	4946.2	6.7	> 10000	7.5
6	> 10000	4349.3	2.1	193.1	56.1
7	3754.6	2220.5	4.7	> 10000	50.0
8	8801.1	3078.3	2.6	> 10000	19.9
9	8921.0	4530.6	7.7	> 10000	50.4
10	> 10000	3007.2	7.5	266.6	6.1
11	4024.3	2470.0	5.3	> 10000	33.2
12	347.6	4033.0	56.8	> 10000	70.4
13	902.4	1718.2	38.4	3763.0	76.3
14	4016.8	2814.2	57.4	15.5	62.8
15	> 10000	4326.1	3.0	> 10000	18.9
16	6459.3	2304.8	2.3	3295.8	22.2
17	7769.6	645.6	8.1	> 10000	35.6
18	3625.7	295.5	6.1	3478.0	66.5
19	3636.7	2556.7	6.3	> 10000	50.3
20	3805.3	2035.7	19.6	> 10000	85.7
21	863.3	7277.8	20.3	11.5	62.1
22	> 10000	4337.9	43.0	244.2	71.2
AAZ	250.0	12.1	6.0	25.8	5.7

* Mean from 3 different assays, by a stopped flow technique (errors were in the range of ± 5–10% of the reported values).

100 nM. In particular, compounds **5** and **10** were as potent as the CAI **AAZ** (K_Is of 7.5, 6.1 and 5.7 nM, respectively). Thus, in consideration of the kinetic data obtained, we focused our attention towards the investigation of the binding modes of our compounds within the hCAs active site with the aim to extract the main structural features responsible of the hCA VII isoform selectivity. In addition, we explored the effects of a selection of such compounds in an oxaliplatin induced model of neuropathic pain.

2.3. Computational studies

With the aim of suggesting a binding mode into hCAs for this class of compounds and analyzing the ligand-protein interaction features that could be at the basis of their selectivity for hCA VII and XII with respect to the other tested hCAs, molecular modeling studies including a robust docking procedure followed by molecular dynamics (MD) simulations in explicit water environment were carried out. Compound **15**, which showed good potency on both hCA VII and XII, was taken into account for this study as a reference ligand of the series. This compound was thus docked into hCA VII using Autodock4 software and the best ranked pose was subjected to 20 ns of MD simulation studies (see the Experimental section for details). As shown in Fig. 3, compound **15** was predicted to chelate the prosthetic zinc ion of hCA VII through the sulfamate group, which also interacted with T201 forming H-bonds with both the backbone nitrogen and the hydroxyl group of the residue. The oxygen atom that connects the sulfamate group with the ureidic fragment showed a stable H-bond with the hydroxyl group of T202, whereas the ureidic carbonyl oxygen formed a water-mediated H-bond with the oxygen backbone of P203. Finally, the 2,5-dimethylphenyl group was found to be localized between N64, Q69, Q94 and F133, thus efficiently blocking the entrance of the binding cavity.

As shown in Fig. SI-1, by superimposing the hCA VII-**15** complex with the starting crystallographic structure of hCA VII used for the analysis (3MDZ PDB code) it is evident that all residues involved in the interaction with the ligand approximately maintained their original disposition, with the exception of N64 and Q69. With regards to N64, the sidechain of the residue showed a different disposition, but the H-bond between its amidic oxygen and the nitrogen backbone of S67 was maintained in both structures. More evident differences can be highlighted for Q69, whose amidic nitrogen was directed towards the water-exposed part of the binding site in the starting crystallographic structure. However, the predicted binding mode of compound **15** is not compatible with this disposition of Q69; in fact, in the hCA VII-**15** complex the presence of the 2,5-dimethylphenyl group forced the sidechain of Q69 to fold towards the protein. This disposition was allowed by the formation of an H-bond between the amidic nitrogen of Q69 and the carboxylic oxygen of D71. Interestingly, an analysis of the conservation of these three residues among the ten most common hCAs reported in this study, highlighted that N64 was conserved in **7** hCAs, Q69 in **4** hCAs, D71 only in two hCAs and the combination of Q69 and D71 was shown only for hCA VII (see Fig. SI-2).

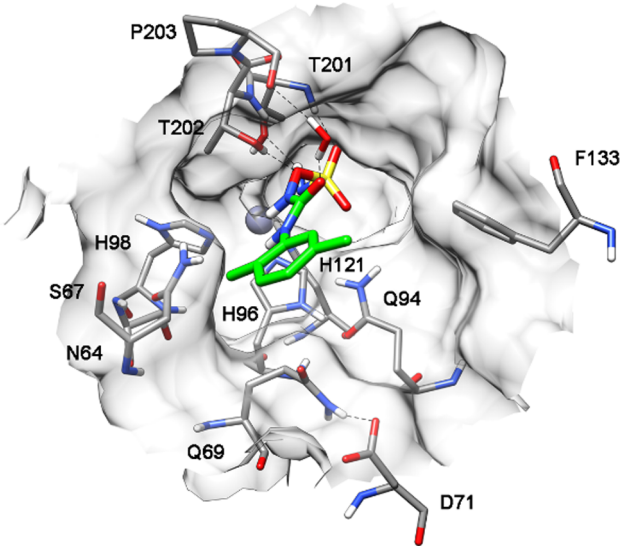

Fig. 3. Predicted binding mode of compound **15** into hCA VII.

In hCA XII, N64 is conserved (N92 for hCA XII) whereas Q69 and D71 are replaced by K97 and N99, respectively. As shown in Fig. 4, the ligand maintained into hCA XII the same binding orientation observed for hCA VII, showing the two interactions of the sulfonamide fragment with T226, the additional H-bond with the hydroxyl group of T227 and the water-mediated H-bond with the oxygen backbone of P228. The

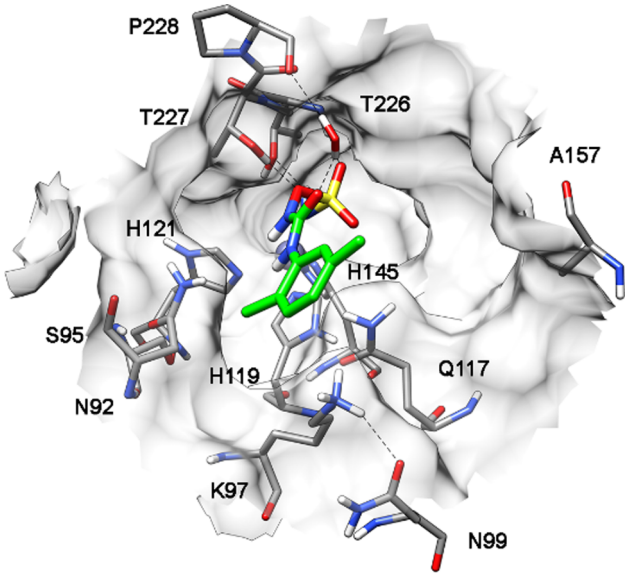

Fig. 4. Predicted binding mode of compound 15 into hCA XII.

conserved residue N92 showed a disposition very similar to that observed for hCA VII and the non-conserved K97 was found to fold towards the protein forming an H-bond with N99, thus allowing the proper disposition of the 2,5-dimethylphenyl group of the ligand within the binding site.

The binding modes predicted for the ligand into the catalytic sites of the other analyzed hCAs were found to be different with respect to those observed into hCA VII and XII. Fig. SI-3A shows the disposition of compound **15** into the binding site of hCA I: the replacement of Q69 present in hCA VII with a histidine residue (H68) prevented the proper orientation of the 2,5-dimethylphenyl group of the ligand, which was instead shifted toward F92 and L132. This disposition allowed the formation of an H-bond between Q93 and a nitrogen of the ureidic fragment of the molecule, but at the same time prevented the ligand sulfonamide moiety to correctly chelate the zinc ion and to form the H-bonds with T200. Furthermore, due to the replacement of T202 with a histidine residue (H201) the ligand also lost the H-bond showed by the oxygen atom that connects the sulfonamide and the ureidic fragment.

The analysis of the interactions of **15** into hCA II binding site highlighted that the non-conserved N67 (Q69 for hCA VII) was not able to fold towards the protein, since it couldn't interact with E69 (D71 for hCA VII) that was involved in a stable ionic interaction with R58. It is interesting to note that the salt bridge between R58 and E69 can be formed only into hCA II, because these two residues are not present into the other hCAs (see Fig. SI-3B). Due to the lack of the interaction between N67 and E69, the asparagine residue was directed towards the water-exposed cavity of the binding site and interacted with the conserved N62, which was thus not able to maintain the disposition showed into hCA VII. On the bases of the different disposition of N62 and N67, the ligand bound to hCA II with the 2,5-dimethylphenyl group occupying the central region of the binding site cavity without forming the two H-bond interactions with T199 and P200, in agreement with the low activity of the compound against this hCA subtype.

In the predicted hCA IX-**15** complex, a further different ligand binding mode was observed. Although in this hCA isoform both N64 and Q69 of hCA VII are conserved (N198 and Q203, respectively, in hCA IX), the threonine residue T205 replacing D71 of hCA VII was not able to establish any H-bond with the conserved Q203 and to allow its folding towards the protein. For this reason, the amide group of Q203 was directed towards the water-exposed region of the binding site, forming stacking interactions with Q224 (Fig. SI-3C). Compound **15** was thus predicted to interact with hCA IX laying its 2,5-dimethylphenyl moiety onto the amide groups of Q203 and Q224; interestingly, the ureidic fragment of the ligand was disposed with the carbonyl oxygen oriented toward H226, in order to form an H-bond with Q224. Although in this case, the ligand was able to properly chelate the zinc ion and to form the H-bond interactions with T332 (T201 in hCA VII) through its sulfonamide moiety, it still lacked the additional H-bond with the hydroxyl group of T333 and the water mediated H-bond with P334 (T202 and P203 in hCA VII, respectively). The lack of these two interactions, which strongly contributed to anchor the ligand to the binding site of hCA VII, may justify its weak inhibitory activity against hCA IX.

2.4. Pain modulating effects of CA inhibitors

Compounds **2**, **6**, **15**, **17–19** with selective inhibitory activities on hCA VII were selected to investigate their neuropathic pain-relieving effects in comparison to the clinically used CAI drug **AAZ** [5,6] in a mice model of neuropathic pain induced by oxaliplatin, [35] an anticancer drug characterized by a relevant neurotoxicity able to induce neuropathy in a high percentage of patients [36,37]. The results are summarized below in Fig. 5.

The pain threshold measurements of oxaliplatin-treated animals (Cold plate test) are shown in Fig. 5. Compound **2** in Fig. 5a, showed a dose dependent pain-relieving effect lasting up to 45 min and peaking at 30 min after administration with both concentrations (e.g. 10 and 30 mg kg^{-1}). An analogous trend was also reported for compound **6** in Fig. 5b. It is worth noting that the introduction in **2** of the chlorine atom at 3-position of the phenyl ring resulted in significative increase of the potency as well as of the biologic effect duration. The comparison of Fig. 5a and b showed that the administration of **6** at a concentration of 3 mg kg^{-1} resulted in a response curve almost superimposable to the one of compound **2** administered at its maximum concentration. Administration of **6** at 30 mg kg^{-1} afforded a response as much intense as the reference **AAZ** at a concentration of 100 mg kg^{-1}. Quite interestingly compound **6** at the range of concentrations used (e.g. 3 to 30 mg kg^{-1}) determined biological responses all peaked at 30 min and lasting up to 60 min after administration (Fig. 5b). The 2,5-dimethylphenyl **15** was slightly more potent when compared to the other non-halogen containing derivative **2** when administered at the maximum concentration (e.g. 30 mg kg^{-1}) and it showed identical time frame efficacy and curve profile (Fig. 5c). The data in Fig. 5d relative to compound **17** do profile for a different type of response depending on the concentration used. For instance, when **17** was administered at 10 mg kg^{-1} the maximum effect was reached just after 15 min from the administration and lasted constant up to 30 min followed by a slow decrement of intensity over 45 min. The use of **17** at a 3-fold higher concentration did result in a constant increase of the biological effect up to 30 min with a value comparable to the reference **AAZ** and then followed by its rapid depletion in just 15 min (Fig. 5d). Again, the introduction of a halogen moiety as in **18**, determined a significative response at the minimal concentration of 3 mg kg^{-1} peaking at 30 min and lasting up to 60 min. The increase of **18** up to 3-fold of the initial concentration resulted in enhancements of the biological effect without any disruption of the curves symmetry (Fig. 5e). The last compound tested showed a weak biological effect when administered at 10 mg kg^{-1}. The increase of its concentration determined a maximum effect at 30 min after administration, with a value over the threshold limit reported for untreated mice used as control. The effected rapidly and constantly diminished up to 60 min after the experiment has started.

The compounds **2**, **6**, **15**, **17–19** were selected for the in vivo testing on the basis of their selectivity profiles against the hCA VII isoform. Any consideration on the solubility of our compounds in water was intentionally skipped since the presence of the *N*'-ureido-*O*-sulfamate moiety is reasonably expected to provide enough hydrophilicity.

3. Conclusions

Here we report for the first time the *N*-phenyl-*N*'-ureido-*O*-sulfamates as a new class of CAIs, designed by merging the ureido, hydroxyurea and hydroxylamine-*O*-sulfonamide chemotypes possessing CA inhibitory effects, in the same molecule. We developed an efficient synthetic procedure which allowed the desired compounds **2–22** in good yields. They were assessed their inhibition properties against several human CAs by means of the stopped flow in vitro assay. Interestingly, the compounds revealed to be effective inhibitors of the hCA isoforms VII and XII with K_I values in the low nanomolar range. In order to determine the binding features at the basis of the selectivity profile of this class of CAIs for the VII and XII isoforms, we carried out molecular modeling studies including a robust docking procedure followed by molecular dynamics (MD) simulations in explicit water environment using compound **15** as a model. Quite interestingly, the superposition of the hCA VII-**15** and hCA XII-**15** complexes revealed closely matching poses, both accounting for a canonical sulfamate coordination of the Zn (II) ion, a strong stabilization of the ureido-*O*-sulfamate section by means of hydrogen bond networks and accommodation of the aryl tail towards the rim of the catalytic cleft. The same compound showed different and less energetically favored poses within the other hCA isoforms studied. Finally, a selection of compounds (e.g. **2**, **6**, **15**, **17–19**) was considered for their neuropathic pain-relieving

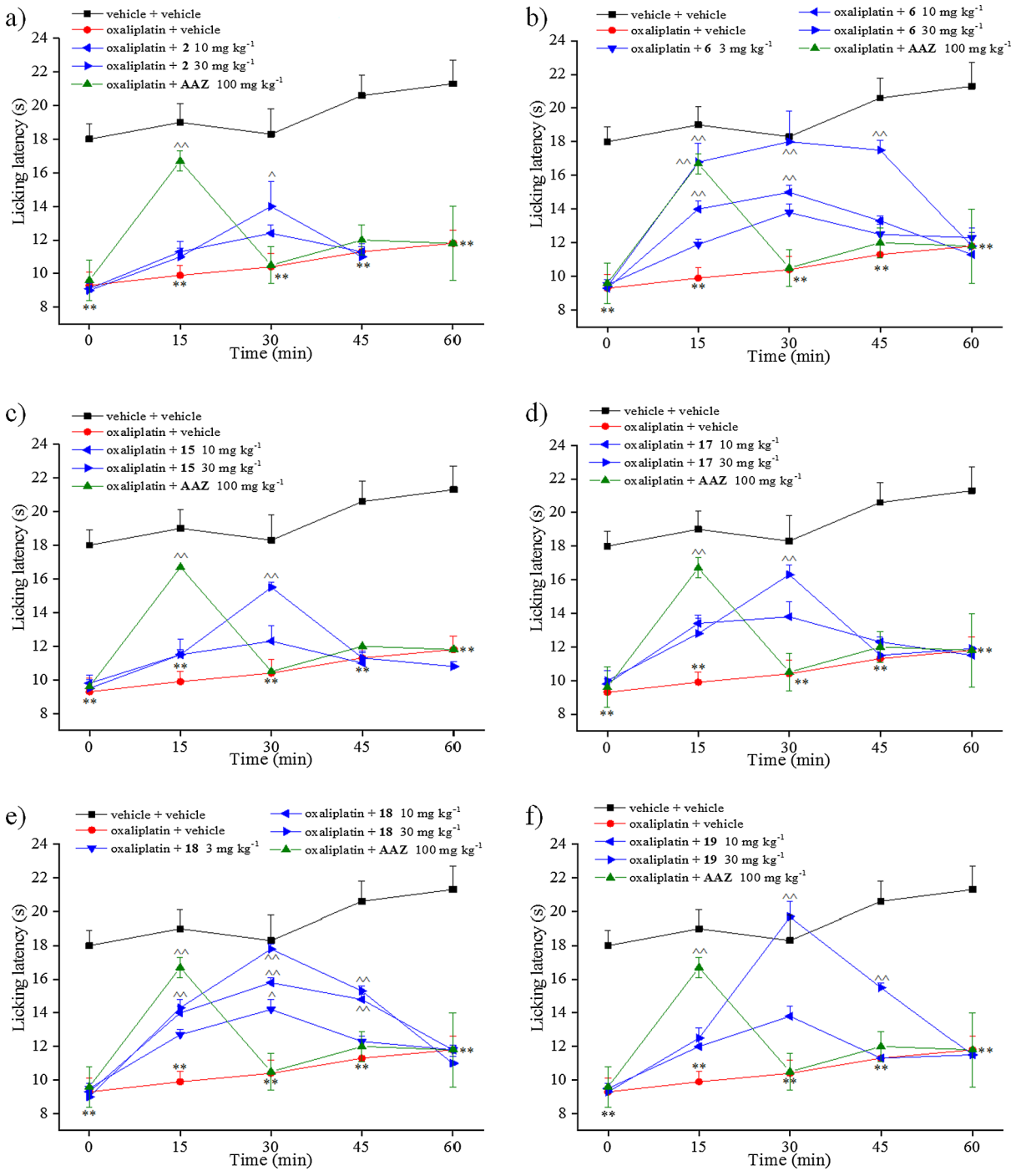

Fig. 5. Graphics are illustrating the modulating effects of CAIs **2** (a), **6** (b), **15** (c), **17** (d), **18** (e) and **19** (f) on neuropathic pain induced by oxaliplatin with comparison to **AAZ**. The response to a thermal stimulus was evaluated by the Cold plate test measuring the latency (s) to pain-related behaviors (lifting or licking of the paw). Mice were treated with oxaliplatin (2.4 mg kg^{-1} i.p.) for two consecutive weeks (10 injections) and the acute tests were performed starting from day 15. Compounds were administered *per o.s.* and the measurements were performed 15, 30, 45 and 60 min after treatments. Control mice were treated only with vehicle. Each value represents the mean of 12 mice per group, performed in 2 different experimental sets. **P < 0.01 *vs* vehicle + vehicle; ^P < 0.05 and ^^P < 0.01 *vs* oxaliplatin + vehicle.

effects in comparison to the clinically used drug **AAZ** in a mice model of neuropathic pain induced by oxaliplatin. All selected compounds showed interesting activities, and among them **6**, **17–19** showed potent analgesic effects. These results give scientific evidence in order to support the *N*-phenyl-*N*'-ureido-*O*-sulfamates as a new and efficient CAI class worth of future development for the obtainment of hCA VII selective inhibitors useful for the management of neuropathic pain.

4. Experimental section

4.1. Materials and methods

Chemistry. All anhydrous solvents and reagents used in this study were purchased from Alfa Aesar, TCI, and Sigma-Aldrich. The synthetic reactions involving air- or moisture-sensitive chemicals were carried out under a nitrogen atmosphere using dried glassware and syringe

techniques in order to transfer the solutions. Nuclear magnetic resonance (^{1}H-, ^{13}C-, and ^{19}F NMR) spectra were recorded using a Bruker Avance III 400 MHz spectrometer using DMSO-d_6 as solvent. The chemical shifts are reported in parts per million (ppm), and the coupling constants (*J*) are expressed in Hertz (Hz). The splitting patterns are designated as s, singlet; d, doublet; t, triplet; q, quartet; m, multiplet; brs, broad singlet; dd, doublet of doublets. The correct assignment of exchangeable protons (i.e., O*H* and N*H*) was carried out by means of the addition of D_2O. Analytical thin-layer chromatography (TLC) was done on Merck silica gel F-254 plates. The HPLC was performed by using a Waters 2690 separation module coupled with a photodiode array detector (PDA Waters 996) using a Nova-Pak C18 4 μm 3.9 mm × 150 mm (Waters) silica-based reverse phase column. The sample was dissolved in 10% acetonitrile/H2O and an injection volume of 45 μL. The mobile phase (flow rate 1.0 mL/min) was a gradient of H2O + trifluoroacetic acid (TFA) 0.1% (A) and acetonitrile + TFA 0.1% (B), with steps as follows: (A%/B%), 0–10 min 90:10, 10–25 min gradient to 60:40, 26:28 min isocratic 20:80, 29–35 min isocratic 90:10. TFA 0.1% in water as well in acetonitrile was used as counterion. All compounds reported here were ≥ 95% HPLC pure. The solvents used in MS measures were acetone, acetonitrile (Chromasolv grade), and mQ water 18 MU. The high resolution mass spectrometry (HRMS) analysis was performed with a Thermo Finnigan LTQ Orbitrap mass spectrometer coupled with an electrospray ionization source (ESI). Analysis was carried out in positive ion mode $[M + H]^+$, and it was used a proper dwell time acquisition to achieve 60,000 units of resolution at full width at half maximum (fwhm). Elemental composition of compounds was calculated on the basis of their measured accurate masses, accepting only results with an attribution error less than 5 ppm and a not integer RDB (double bond/ring equivalents) value [32] tock solutions of analytes were prepared using acetone (1.0 mg mL^{-1}) and stored at 4 °C. Then working solutions of each analyte were prepared by dilution of the stock solutions using mQ H_2O/ACN 1/1 (*v/v*) up to a concentration of 1.0 μg mL^{-1}. The HRMS analysis was performed by introducing the analyte working solution via syringe pump at 10 μL min^{-1}.

4.2. Synthesis of compounds

A solution of hydroxyureas **2a-22a** [33] (0.2 g, 1.0 eq) in dry DMA at 0 °C was treated with freshly prepared sulfamoylchloride (6.0 eq, portion-wise). The reaction mixture was warmed to rt and stirred for 15 min then quenched with slush. The obtained precipitate was filtered-off and washed with DCM (3 × 5 mL) to afford desired products **7, 13, 15–16, 18, 21**. Alternatively the mixture was extracted with ethyl acetate (3 × 15 mL). The combined organic layers were washed with brine (3 × 15 mL), dried over anhydrous Na_2SO_4, filtered and the solvents were removed under vacuum to afford desired product **2–6, 8–12, 14, 17, 19, 20, 22**.

4.2.1. S-((3-phenylureido)oxy)sulfonamide (2)

Brown solid, 75% yield; mp 123–124 °C (dec); δ_H (400 MHz, DMSO-d_6) 7.08 (1H, t, *J* 7.6), 7.34 (2H, t, *J* 7.6), 7.57 (2H, d, *J* 7.6), 8.00 (2H, s, exchange with D_2O, SO_2NH_2), 8.84 (1H, s, exchange with D_2O, NH), 10.50 (1H, s, exchange with D_2O, NH); δ_C (100 MHz, DMSO-d_6) 120.9, 124.1, 129.5, 139.3, 156.9; HRMS *m/z* $[M-H]^-$ calcd for C7H9N3O4S, 231,0314; found, 231,0311.

4.2.2. S-((3-(p-Tolyl)ureido)oxy)sulfonamide (3)

Pale yellow solid, 88% yield; mp 143–144 °C (dec); δ_H (400 MHz, DMSO-d_6) 2.29 (3H, s), 7.14 (2H, d, *J* 8.0), 7.44 (2H, d, *J* 8.0), 7.98 (2H, s, exchange with D_2O, SO_2NH_2), 8.73 (1H, s, exchange with D_2O, NH), 10.44 (1H, s, exchange with D_2O, NH); δ_C (100 MHz, DMSO-d_6) 21.3, 120.9, 129.9, 133.0, 136.6, 156.9; HRMS *m/z* $[M-H]_-$ calcd for C8H11N3O4S, 245,0470; found, 245,04685.

4.2.3. S-((3-(o-Tolyl)ureido)oxy)sulfonamide (4)

Pale yellow solid, 45% yield; mp 141–142 °C (dec); δ_H (400 MHz, DMSO-d_6) 2.24 (3H, s), 7.13 (1H, t, *J* 7.6), 7.22 (1H, t, *J* 7.6), 7.26 (1H, d, *J* 7.6), 7.47 (1H, d, *J* 7.6), 8.07 (2H, s, exchange with D_2O, SO_2NH_2), 8.24 (1H, s, exchange with D_2O, NH), 10.53 (1H, s, exchange with D_2O, NH); δ_C (100 MHz, DMSO-d_6) 18.5, 125.5, 126.0, 127.1, 131.2, 132.6, 136.6, 157.3; HRMS *m/z* $[M-H]^-$ calcd for C8H11N3O4S, 244,0470; found, 244,0474.

4.2.4. S-((3-(4-chlorophenyl)ureido)oxy)sulfonamide (5)

Pale yellow solid, 52% yield; mp 172–173 (dec) °C; δ_H (400 MHz, DMSO-d_6) 7.39 (2H, d, *J* 8.8), 7.61 (2H, d, *J* 8.8), 8.00 (2H, s, exchange with D_2O, SO_2NH_2), 9.05 (1H, s, exchange with D_2O, NH), 10.61 (1H, s, exchange with D_2O, NH); δ_C (100 MHz, DMSO-d_6) 122.3, 127.7, 129.4, 138.4, 156.8; HRMS *m/z* $[M-H]^-$ calcd for C7H8ClN3O4S, 263,9924; found, 263,9920.

4.2.5. S-((3-(3-Chlorophenyl)ureido)oxy)sulfonamide (6)

Pale yellow solid, 70% yield; mp 175–176 °C (dec); δ_H (400 MHz, DMSO-d_6) 7.13 (1H, ddd, *J* 0.92, 2.04, 8.0), 7.36 (1H, t, *J* 8.0), 7.54 (1H, ddd, *J* 0.92, 2.04, 8.0), 7.75 (1H, t, *J* 2.04), 8.02 (2H, s, exchange with D_2O, SO_2NH_2), 9.12 (1H, s, exchange with D_2O, NH), 10.68 (1H, s, exchange with D_2O, NH); δ_C (100 MHz, DMSO-d_6) 119.1, 120.1, 123.6, 131.2, 133.9, 141.0, 156.8; HRMS *m/z* $[M-H]^-$ calcd for C7H8ClN3O4S, 263,9924; found, 263,9927.

4.2.6. S-((3-(2-chlorophenyl)ureido)oxy)sulfonamide (7)

Pale yellow solid, 71% yield; mp 172–173 °C (dec); δ_H (400 MHz, DMSO-d_6) 7.20 (1H, t, *J* 8.0), 7.38 (1H, t, *J* 8.0), 7.54 (1H, d, *J* 8.0), 7.92 (1H, d, *J* 8.0), 8.20 (2H, s, exchange with D_2O, SO_2NH_2), 8.38 (1H, exchange with D_2O, NH), 10.84 (1H, s, exchange with D_2O, NH); δ_C (100 MHz, DMSO-d_6) 124.4, 125.7, 126.3, 128.6, 130.3, 135.3, 156.5; HRMS *m/z* $[M-H]^-$ calcd for C7H8ClN3O4S, 263,9924; found, 263,9922

4.2.7. S-((3-(4-fluorophenyl)ureido)oxy)sulfonamide (8)

Pale yellow, 37% yield; mp 162–163 °C (dec); δ_H (400 MHz, DMSO-d_6) 7.18 (2H, m), 7.58 (2H, m), 7.99 (2H, s, exchange with D_2O, SO_2NH_2), 8.94 (1H, s, exchange with D_2O, NH), 10.55 (1H, s, exchange with D_2O, NH); δ_C (100 MHz, DMSO-d_6) 116.0 (d, $^{2}J_{C\text{-}F}$ 22), 122.8 (d, $^{3}J_{C\text{-}F}$ 7), 135.6 (d, $^{4}J_{C\text{-}F}$ 2), 157.0, 159.0 (d, $^{1}J_{C\text{-}F}$ 238); δ_F (376 MHz, DMSO-d_6) −119.9 (1F, s); HRMS *m/z* $[M-H]^-$ calcd for C7H8FN3O4S, 249,0220; found, 249,0223.

4.2.8. S-((3-(4-nitrophenyl)ureido)oxy)sulfonamide (9)

Yellow solid, 60% yield; mp 170–171 °C (dec); δ_H (400 MHz, DMSO-d_6) 7.86 (2H, d, *J* 9.2), 8.07 (2H, s, exchange with D_2O, SO_2NH_2), 8.25 (2H, d, *J* 9.2), 9.66 (1H, s, exchange with D_2O, NH), 10.88 (1H, s, exchange with D_2O, NH); δ_C (100 MHz, DMSO-d_6) 119.9, 125.7, 142.9, 146.2, 156.4; HRMS *m/z* $[M-H]^-$ calcd for C7H8N4O6S, 276,0165; found, 276,0168.

4.2.9. S-((3-(2-nitrophenyl)ureido)oxy)sulfonamide (10)

Yellow solid, 57% yield; mp 136–137 °C (dec); δ_H (400 MHz, DMSO-d_6) 7.34 (1H, t, *J* 8.0), 7.79 (1H, t, *J* 8.0), 8.19 (1H, d, *J* 8.0), 8.23 (2H, s, exchange with D_2O, SO_2NH_2), 8.31 (1H, d, *J* 8.0), 10.05 (1H, s, exchange with D_2O, NH), 11.24 (1H, s, exchange with D_2O, NH); δ_C (100 MHz, DMSO-d_6) 123.3, 124.5, 126.5, 134.4, 136.3, 139.1, 156.2; HRMS *m/z* $[M-H]^-$ calcd for C7H8N4O6S, 276,0165; found, 276,0169.

4.2.10. S-((3-(2-methoxyphenyl)ureido)oxy)sulfonamide (11)

White solid, 31% yield; mp 167–168 °C (dec); δ_H (400 MHz, DMSO-d_6) 3.89 (3H, s), 6.93–7.00 (1H, m), 7.09 (2H, m), 7.97 (1H, d, *J* 7.6), 8.17 (1H, s, exchange with D_2O, NH), 8.21 (2H, s, exchange with D_2O, SO_2NH_2), 10.67 (1H, s, exchange with D_2O, NH); δ_C (100 MHz,

DMSO-d_6) 56.8, 112.0, 120.3, 121.4, 124.5, 127.8, 149.5, 156.4; HRMS m/z $[M-H]^-$ calcd for C8H11N3O5S, 261,0419; found, 261,0422.

*4.2.11. S-((3-(2-ethoxyphenyl)ureido)oxy)sulfonamide (**12**)*

White solid, 85% yield; mp 160–161 °C (dec); δ_H (400 MHz, DMSO-d_6) 1.41 (3H, t, J 7.0), 4.13 (2H, q, J 7.0), 6.95 (1H, m), 7.05 (2H, m), 8.02 (1H, dd, J 1.2, 8.0), 8.22 (3H, m, exchange with D_2O, NH and SO_2NH_2), 10.71 (1H, s, exchange with D_2O, NH); δ_C (100 MHz, DMSO-d_6) 15.8, 65.6, 113.4, 120.2, 121.9, 125.0, 128.2, 148.9, 157.0; HRMS m/z $[M-H]^-$ calcd for C9H13N3O5S, 275,0576; found, 275,0567.

*4.2.12. S-((3-(4-phenoxyphenyl)ureido)oxy)sulfonamide (**13**)*

White solid, 60% yield; mp 152–153 °C (dec); δ_H (400 MHz, DMSO-d_6) 7.01 (4H, m), 7.14 (1H, t, J 8.0), 7.40 (2H, t, J 8.0), 7.59 (2H, d, J 8.8), 8.02 (2H, s, exchange with D_2O, SO_2NH_2), 8.93 (1H, s, exchange with D_2O, NH), 10.53 (1H, s, exchange with D_2O, NH); δ_C (100 MHz, DMSO-d_6) 118.8, 120.3, 122.7, 123.9, 130.9, 135.1, 152.7, 157.0, 158.3; HRMS m/z $[M-H]^-$ calcd for C13H13N3O5S, 323,0576; found, 323,0575.

*4.2.13. Ethyl 3-(3-(sulfamoyloxy)ureido)benzoate (**14**)*

Pale yellow solid, 70% yield; mp 151–152 °C (dec); δ_H (400 MHz, DMSO-d_6) 1.36 (3H, t, J 7.2), 4.35 (2H, q, J 7.2), 7.49 (1H, t, J 8.0), 7.67 (1H, m), 7.89 (1H, m), 8.01 (2H, s, exchange with D_2O, SO_2NH_2), 8.23 (1H, t, J 2.0), 9.16 (1H, s, exchange with D_2O, NH), 10.65 (1H, s, exchange with D_2O, NH); δ_C (100 MHz, DMSO-d_6) 15.1, 61.7, 121.3, 124.6, 125.2, 129.9, 131.2, 139.8, 156.9, 166.5; HRMS m/z $[M-H]^-$ calcd for C10H13N3O6S, 303,0525; found, 303,0522.

*4.2.14. S-((3-(2,5-dimethylphenyl)ureido)oxy)sulfonamide (**15**)*

White solid 50% yield; mp 157–158 °C (dec); δ_H (400 MHz, DMSO-d_6) 2.19 (3H, s), 2.29 (3H, s), 6.94 (1H, d, J 7.6), 7.13 (1H, d, J 7.6), 7.30 (1H, s), 8.06 (2H, s, exchange with D_2O, SO_2NH_2), 8.17 (1H, s, exchange with D_2O, NH), 10.51 (1H, s, exchange with D_2O, NH); δ_C (100 MHz, DMSO-d_6) 18.0, 21.5, 125.9, 126.6, 129.3, 131.0, 136.1, 136.4, 157.2; HRMS m/z $[M-H]^-$ calcd for C9H13N3O4S, 259,0627; found, 259,0625.

*4.2.15. S-((3-(3,5-dimethylphenyl)ureido)oxy)sulfonamide (**16**)*

White solid, 75% yield; mp 160–161 °C (dec); δ_H (400 MHz, DMSO-d_6) 2.27 (6H, s), 6.73 (1H, s), 7.20 (2H, s), 8.00 (2H, s, exchange with D_2O, SO_2NH_2), 8.63 (1H, s, exchange with D_2O, NH), 10.46 (1H, s, exchange with D_2O, NH); δ_C (100 MHz, DMSO-d_6) 22.0, 118.5, 125.7, 138.5, 139.1, 156.8; HRMS m/z $[M-H]^-$ calcd for C9H13N3O4S, 259,0627; found, 259,0631.

*4.2.16. S-((3-(4-(trifluoromethyl)phenyl)ureido)oxy)sulfonamide (**17**)*

Pale yellow solid, 88% yield; mp 149–150 °C (dec); δ_H (400 MHz, DMSO-d_6) 7.70 (2H, d, J 8.8), 7.81 (2H, d, J 8.8), 8.04 (2H, s, exchange with D_2O, SO_2NH_2), 9.33 (1H, s, exchange with D_2O, NH), 10.73 (1H, s, exchange with D_2O, NH); δ_C (100 MHz, DMSO-d_6) 120.4, 124.0 (q, $^2J_{C-F}$ 32), 125.4 (q, $^1J_{C-F}$ 270), 126.8 (q, $^3J_{C-F}$ 4), 143.3 (q, $^4J_{C-F}$ 1), 156.7; δ_F (376 MHz, DMSO-d_6) −60.2 (3F, s); HRMS m/z $[M-H]^-$ calcd for C8H8F3N3O4S, 299,0188; found, 299,0190.

*4.2.17. S-((3-(4-fluoro-3-methylphenyl)ureido)oxy)sulfonamide (**18**)*

White solid, 45% yield; mp 157–158 °C (dec); δ_H (400 MHz, DMSO-d_6) 2.24 (3H, d, J 1.6), 7.11 (1H, m), 7.39–7.47 (2H, m), 7.99 (2H, s, exchange with D_2O, SO_2NH_2), 8.83 (1H, exchange with D_2O, NH), 10.53 (1H, s, exchange with D_2O, NH); δ_C (100 MHz, DMSO-d_6) 15.2 (d, J_{C-F} 3), 115.7 (d, J_{C-F} 23), 120.1 (d, J_{C-F} 8), 124.0 (d, J_{C-F} 5), 125.0 (d, J_{C-F} 18), 135.2 (d, J_{C-F} 3), 157.0, 157.6 (d, J_{C-F} 237); δ_F (376 MHz, DMSO-d_6) −124.2 (1F, s); HRMS m/z $[M-H]^-$ calcd for C8H10FN3O4S, 263,0376; found, 263,0378.

*4.2.18. S-((3-(2-chloro-4-(trifluoromethyl)phenyl)ureido)oxy)sulfonamide (**19**)*

White solid, 57% yield; mp 159–160 °C (dec); δ_H (400 MHz, DMSO-d_6) 7.78 (1H, dd, J 1.6, 8.8), 7.97 (1H, d, J 1.6), 8.26 (1H, d, J 8.8), 8.28 (2H, s, exchange with D_2O, SO_2NH_2), 8.58 (1H, exchange with D_2O, NH), 11.07 (1H, s, exchange with D_2O, NH); δ_C (100 MHz, DMSO-d_6) 123.0, 124.4 (q, J_{C-F} 270), 124.8, 125.5 (q, J_{C-F} 33), 125.9 (q, J_{C-F} 4), 127.4 (q, J_{C-F} 4), 139.3 (q, J_{C-F} 1), 155.9; δ_F (376 MHz, DMSO-d_6) −60.6 (3F, s); HRMS m/z $[M-H]^-$ calcd for C8H7ClF3N3O4S, 332,9798; found, 332,9796

*4.2.19. S-((3-(perfluorophenyl)ureido)oxy)sulfonamide (**20**)*

White solid, 64% yield; mp 168–169 °C (dec); δ_H (400 MHz, DMSO-d_6) 8.07 (2H, s, exchange with D_2O, SO_2NH_2), 9.15 (1H, s, exchange with D_2O, NH), 11.00 (1H, s, exchange with D_2O, NH); δ_C (100 MHz, DMSO-d_6) 113.8 (t, J_{C-F} 15), 138.1 (m, J_{C-F} 248), 140.1 (m, J_{C-F} 244), 144.3 (m, J_{C-F} 248), 157.0; δ_F (376 MHz, DMSO-d_6) 163.7 (2F, dt, J_{C-F} 4.9, 22.9), 157.6 (1F, t, J_{C-F} 22.9), 145.6 (2F, dd, J_{C-F} 4.9, 22.9); HRMS m/z $[M-H]^-$ calcd for C7H4F5N3O4S, 320,9843; found, 320,9845.

*4.2.20. S-((3-(2,3-dihydro-1H-inden-5-yl)ureido)oxy)sulfonamide (**21**)*

White solid, 61% yield; mp 149–150 °C (dec); δ_H (400 MHz, DMSO-d_6) 2.04 (2H, m), 2.85 (4H, m), 7.17 (1H, d, J 8.0), 7.28 (1H, dd, J 2.0, 8.0), 7.44 (1H, d, J 2.0), 7.99 (2H, s, exchange with D_2O, SO_2NH_2), 8.69 (1H, s, exchange with D_2O, NH), 10.43 (1H, s, exchange with D_2O, NH); δ_C (100 MHz, DMSO-d_6) 26.1, 32.7, 33.4, 117.2, 119.1, 124.9, 137.3, 139.4, 145.0, 156.9; HRMS m/z $[M-H]^-$ calcd for C10H13N3O4S, 271,0627; found, 271,0629.

*4.2.21. S-((3-(naphthalen-1-yl)ureido)oxy)sulfonamide (**22**)*

White solid, 65% yield; mp 217–218 °C (dec); δ_H (400 MHz, DMSO-d_6) 7.53–7.65 (4H, m), 7.84 (1H, d, J 8.4), 7.98–8.06 (2H, m), 8.11 (2H, s, exchange with D_2O, SO_2NH_2), 8.97 (1H, s, exchange with D_2O, NH), 10.65 (1H, s, exchange with D_2O, NH); δ_C (100 MHz, DMSO-d_6) 123.4, 123.6, 126.5, 126.6, 126.9, 127.1, 129.1, 129.6, 133.9, 134.7, 158.0; HRMS m/z $[M-H]^-$ calcd for C11H11N3O4S, 281,0470; found, 281,0472.

4.3. In vitro Carbonic Anhydrase inhibition assay

The CA-catalyzed CO_2 hydration activity was performed on an Applied Photophysics stopped-flow instrument using phenol red (at a concentration of 0.2 mM) as a pH indicator with 20 mM Hepes (pH 7.5) as the buffer, 20 mM Na_2SO_4, and following the initial rates of the CA-catalyzed CO_2 hydration reaction for a period of 10–100 s and working at the maximum absorbance of 557 nm [38,39]. The CO_2 concentrations ranged from 1.7 to 17 mM. For each inhibitor six traces of the initial 5–10% of the reaction have been used in order to determine the initial velocity. The uncatalyzed reaction rates were determined in the same manner and subtracted from the total observed rates. Stock solutions of inhibitor (0.1 mM) were prepared in distilled water, and dilutions up to 0.01 nM were prepared. Solutions containing inhibitor and enzyme were preincubated for 15 min at room temperature prior to assay in order to allow the formation of the E–I complex. The inhibition constants were obtained as nonlinear least-squares protocols using PRISM 3 38,39 and are the mean from at least three different measurements. All hCAs were recombinant ones and were obtained in house [38,39].

4.4. Molecular docking

The crystal structures of hCA I (PDB code 1AZM), hCA II (PDB code 2AW1), hCA VII (PDB code 3MDZ), hCA IX (PDB code 3IAI) and hCA XII (PDB code 1JD0) were taken from the Protein Data Bank [40]. Molecular docking calculations were performed with Autodock 4.2 [41]

using the improved force field [42,43]. Autodock Tools were employed for identifying the torsion angles in the ligands, add the solvent model and assign the Kollman atomic charges to the proteins. Ligand charges were calculated with the Gasteiger method. A grid spacing of 0.375 Å and a distance-dependent function of the dielectric constant were used for the calculation of the energetic maps, generated within a grid box including all protein residues located in a shell of 10 Å from the bound ligand. The ligand was subjected to a docking procedure already used in pose prediction studies [44,45]. The docked compound was subjected to 200 runs of the Autodock search using the Lamarckian Genetic Algorithm, performing 10 000 000 steps of energy evaluation. For each docking run, a maximum of 10 000 000 generations were simulated starting from an initial population of 500 individuals. The docking solutions were clustered using an rms threshold of 2.0 Å. All other settings were left as their defaults and the best docked conformation was taken into account.

Molecular dynamics simulations. The ligand-protein complexes generated by docking compound **15** into the catalytic sites of the five different hCA isoforms were studied through molecular dynamic (MD) simulations with AMBER [46]. Each complex was subjected to an MD procedure based on an already successfully applied protocol, using the ff14SB force field at 300 K [47]. Prior to MD simulations, each complex was placed in a rectangular parallelepiped water box and solvated with a 20 Å water cap using TIP3P explicit solvent model for water. Sodium or chlorine ions were then added as counterions for the neutralization of the solvated system. Each system was subjected to two stages of energy minimization, each composed of 5000 steps of steepest descent followed by conjugate gradient until a convergence of 0.05 kcal/(mol ± 2) was reached. In the first stage, the whole protein was blocked with a position restraint of 500 kcal/(mol ± 2) to uniquely minimize the position of the water molecules, while in the second stage the entire system was energy minimized applying a harmonic potential of 10 kcal/(mol ± 2) only to the protein α carbons. The minimized complexes were then used as the starting point for a total of 20 ns of MD simulation. A 0.5 ns constant-volume simulation, in which the temperature of the system was raised from 0 to 300 K, was initially performed. In the second step, the system was equilibrated through a 3 ns constant-pressure simulation, maintaining the temperature at the constant value of 300 K with the use of Langevin thermostat. Additional 16.5 ns of constant-pressure MD were then performed, for a total of 20 ns of simulation. In all three MD steps, a harmonic potential of 10 kcal/(mol ± 2) was applied to the protein α carbons. All simulations were performed using particle mesh Ewald (PME) electrostatics with a cutoff of 10 Å for non-bonded interactions and periodic boundary conditions. A simulation step of 2.0 fs was employed, as all bonds involving hydrogen atoms were kept rigid using SHAKE algorithm. General Amber force field (GAFF) parameters were used for the ligand, whose partial charges were calculated with the AM1-BCC method as implemented in the Antechamber suite of AMBER 16.

4.5. Animals

Male CD-1 albino mice (Envigo, Varese, Italy) weighing approximately 22–25 g at the beginning of the experimental procedure, were used. Animals were housed in Ce.S.A.L (Centro Stabulazione Animali da Laboratorio, University of Florence) and used at least 1 week after their arrival. Ten mice were housed per cage (size 26 × 41 cm). Animals were fed a standard laboratory diet and tap water ad libitum, and kept at 23 ± 1 °C with a 12 h light/dark cycle, light at 7 a.m. All animal manipulations were carried out according to the Directive 2010/63/EU of the European parliament and of the European Union council (22 September 2010) on the protection of animals used for scientific purposes. The ethical policy of the University of Florence complies with the Guide for the Care and Use of Laboratory Animals of the US National Institutes of Health (NIH Publication No. 85–23, revised 1996; University of Florence assurance number: A5278-01). Formal approval to conduct the experiments described was obtained from the Animal Subjects Review Board of the University of Florence. Experiments involving animals have been reported according to ARRIVE guideline [48]. All efforts were made to minimize animal suffering and to reduce the number of animals used.

4.5.1. Oxaliplatin-induced neuropathic pain model and pharmacological treatments

Mice treated with oxaliplatin (2.4 mg·kg-1) were administered intraperitoneally (i.p.) on days 1–2, 5–9, 12–14 (10 i.p. injections) [35,49]. Oxaliplatin was dissolved in 5% glucose solution. Control animals received an equivalent volume of vehicle. Behavioural tests were performed starting from day 15. **AAZ** (100 mg·kg-1) and **2, 6, 15, 17–19** (3–30 mg kg^{-1}) were suspended in 1% carboxymethylcellulose sodium salt (CMC, Sigma-Aldrich, Milan, Italy) and per os (p.o.) acutely administered.

4.5.2. Cold plate test

The animals were placed in a stainless steel box (12 cm × 20 cm × 10 cm) with a cold plate as floor. The temperature of the cold plate was kept constant at 4 °C ± 1 °C. Pain-related behaviour (licking of the hind paw) was observed and the time (seconds) of the first sign was recorded. The cut-off time of the latency of paw lifting or licking was set at 60 s [50,51].

4.5.3. Statistical analysis

Behavioural measurements were performed on 12 mice for each treatment carried out in 2 different experimental sets. Results were expressed as mean ± S.E.M. The analysis of variance of behavioural data was performed by one way ANOVA, a Bonferroni's significant difference procedure was used as post-hoc comparison. P values of less than 0.05 or 0.01 were considered significant. Investigators were blind to all experimental procedures. Data were analysed using the "Origin 9" software (OriginLab, Northampton, USA).

Appendix A. Supplementary material

Supplementary data to this article can be found online at https://doi.org/10.1016/j.bioorg.2019.103033.

References

[1] T. Jensen, R. Baron, M. Haanpää, E. Kalso, J. Loeser, A. Rice, R.-D. Treede, A new definition of neuropathic pain, Pain 152 (2011) 2204–2205.
[2] N.B. Finnerup, S. Haroutounian, P. Kamerman, R. Baron, D.L.H. Bennett, D. Bouhassira, G. Cruccu, R. Freeman, P. Hansson, T. Nurmikko, et al., Neuropathic pain: an updated grading system for research and clinical practice, Pain 157 (2016) 1599–1606.
[3] M. Asiedu, M.H. Ossipov, K. Kaila, T.J. Price, Acetazolamide and midazolam act synergistically to inhibit neuropathic pain, Pain 148 (2010) 302–308.
[4] M.N. Asiedu, G.L. Mejia, C.A. Hübner, K. Kaila, T.J. Price, Inhibition of carbonic anhydrase augments GABAA receptor-mediated analgesia via a spinal mechanism of action, J. Pain 15 (2014) 395–406.
[5] F. Carta, L. Di Cesare Mannelli, M. Pinard, C. Ghelardini, A. Scozzafava, R. McKenna, C.T. Supuran, A class of sulfonamide carbonic anhydrase inhibitors with neuropathic pain modulating effects, Bioorg. Med. Chem. 23 (2015) 1828–1840.
[6] A. Angeli, L. Di Cesare Mannelli, E. Lucarini, T.S. Peat, C. Ghelardini, C.T. Supuran, Design, synthesis and X-Ray crystallography of selenides bearing benzenesulfonamide moiety with neuropathic pain modulating effects, Eur. J. Med. Chem. 154 (2018) 210–219.
[7] C.T. Supuran, Carbonic Anhydrase inhibition and the management of neuropathic pain, Expert Rev. Neurother. 16 (2016) 961–968.
[8] C.T. Supuran, Carbonic Anhydrases: novel therapeutic applications for inhibitors and activators, Nat. Rev. Drug Discov. 7 (2008) 168–181.
[9] A. Maresca, C. Temperini, H. Vu, N.B. Pham, S.-A. Poulsen, A. Scozzafava, R.J. Quinn, C.T. Supuran, Non-zinc mediated inhibition of carbonic anhydrases: coumarins are a new class of suicide inhibitors, J. Am. Chem. Soc. 131 (2009) 3057–3062.
[10] A. Maresca, C. Temperini, L. Pochet, B. Masereel, A. Scozzafava, C.T. Supuran, Deciphering the mechanism of carbonic anhydrase inhibition with coumarins and thiocoumarins, J. Med. Chem. 53 (2010) 335–344.
[11] M. Ferraroni, F. Carta, A. Scozzafava, C.T. Supuran, Thioxocoumarins show an

alternative carbonic anhydrase inhibition mechanism compared to coumarins, J. Med. Chem. 59 (2016) 462–473.
[12] N. Touisni, A. Maresca, P.C. McDonald, Y. Lou, A. Scozzafava, S. Dedhar, J.-Y. Winum, C.T. Supuran, Glycosyl coumarin Carbonic Anhydrase IX and XII inhibitors strongly attenuate the growth of primary breast tumors, J. Med. Chem. 54 (2011) 8271–8277.
[13] A. Bonneau, A. Maresca, J.-Y. Winum, C.T. Supuran, Metronidazole-coumarin conjugates and 3-cyano-7-hydroxy-coumarin act as isoform-selective Carbonic Anhydrase Inhibitors, J. Enzyme Inhib. Med. Chem. 28 (2013) 397–401.
[14] A. Sharma, M. Tiwari, C.T. Supuran, Novel coumarins and benzocoumarins acting as isoform-selective inhibitors against the tumor-associated Carbonic Anhydrase IX, J. Enzyme Inhib. Med. Chem. 29 (2014) 292–296.
[15] K. Tars, D. Vullo, A. Kazaks, J. Leitans, A. Lends, A. Grandane, R. Zalubovskis, A. Scozzafava, C.T. Supuran, Sulfocoumarins (1,2-benzoxathiine-2,2-dioxides): a class of potent and isoform-selective inhibitors of tumor-associated Carbonic Anhydrases, J. Med. Chem. 56 (2013) 293–300.
[16] M. Tanc, F. Carta, M. Bozdag, A. Scozzafava, C.T. Supuran, 7-Substituted-sulfocoumarins are isoform-selective, potent Carbonic Anhydrase II Inhibitors, Bioorg. Med. Chem. 21 (2013) 4502–4510.
[17] A. Innocenti, S.B. Sarıkaya, I. Gülçin, C.T. Supuran, Carbonic Anhydrase Inhibitors. Inhibition of mammalian isoforms I-XIV with a series of natural product polyphenols and phenolic acids, Bioorg. Med. Chem. 18 (2010) 2159–2164.
[18] F. Carta, C. Temperini, A. Innocenti, A. Scozzafava, K. Kaila, C.T. Supuran, Polyamines inhibit Carbonic Anhydrases by anchoring to the zinc-coordinated water molecule, J. Med. Chem. 53 (2010) 5511–5522.
[19] F. Carta, M. Aggarwal, A. Maresca, A. Scozzafava, R. McKenna, E. Masini, C.T. Supuran, Dithiocarbamates strongly inhibit Carbonic Anhydrases and show antiglaucoma action in vivo, J. Med. Chem. 55 (2012) 1721–1730.
[20] F. Carta, M. Aggarwal, A. Maresca, A. Scozzafava, R. McKenna, C.T. Supuran, Dithiocarbamates: a new class of Carbonic Anhydrase Inhibitors. Crystallographic and kinetic investigations, Chem. Commun. (Camb.) 48 (2012) 1868–1870.
[21] F. Carta, A. Akdemir, A. Scozzafava, E. Masini, C.T. Supuran, Xanthates and trithiocarbonates strongly inhibit Carbonic Anhydrases and show antiglaucoma effects in vivo, J. Med. Chem. 56 (2013) 4691–4700.
[22] D. Vullo, M. Durante, F.S. Di Leva, S. Cosconati, E. Masini, A. Scozzafava, E. Novellino, C.T. Supuran, F. Carta, Monothiocarbamates strongly inhibit Carbonic Anhydrases in vitro and possess intraocular pressure lowering activity in an animal model of glaucoma, J. Med. Chem. 59 (2016) 5857–5867.
[23] K. D'Ambrosio, S. Carradori, S.M. Monti, M. Buonanno, D. Secci, D. Vullo, C.T. Supuran, G. De Simone, Out of the active site binding pocket for Carbonic Anhydrase Inhibitors, Chem. Commun. (Camb.) 51 (2015) 302–305.
[24] V. Alterio, R. Cadoni, D. Esposito, D. Vullo, A.D. Fiore, S.M. Monti, A. Caporale, M. Ruvo, M. Sechi, P. Dumy, et al., Benzoxaborole as a new chemotype for Carbonic Anhydrase Inhibition, Chem. Commun. (Camb.) 52 (2016) 11983–11986.
[25] A. Angeli, D. Tanini, A. Nocentini, A. Capperucci, M. Ferraroni, P. Gratteri, C.T. Supuran, Selenols: a new class of Carbonic Anhydrase Inhibitors, Chem. Commun. (Camb.) 55 (2019) 648–651.
[26] C. Temperini, A. Innocenti, A. Scozzafava, C.T. Supuran, N-Hydroxyurea–a versatile zinc binding function in the design of metalloenzyme inhibitors, Bioorg. Med. Chem. Lett. 16 (2006) 4316–4320.
[27] F. Pacchiano, M. Aggarwal, B.S. Avvaru, A.H. Robbins, A. Scozzafava, R. McKenna, C.T. Supuran, Selective hydrophobic pocket binding observed within the Carbonic Anhydrase II active site accommodate different 4-substituted-ureido-benzenesulfonamides and correlate to inhibitor potency, Chem. Commun. (Camb.) 46 (2010) 8371–8373.
[28] F. Pacchiano, F. Carta, P.C. McDonald, Y. Lou, D. Vullo, A. Scozzafava, S. Dedhar, C.T. Supuran, Ureido-substituted benzenesulfonamides potently inhibit Carbonic Anhydrase IX and show antimetastatic activity in a model of breast cancer metastasis, J. Med. Chem. 54 (2011) 1896–1902.
[29] Y. Lou, P.C. McDonald, A. Oloumi, S. Chia, C. Ostlund, A. Ahmadi, A. Kyle, U. Auf dem Keller, S. Leung, D. Huntsman, et al., Targeting tumor hypoxia: suppression of breast tumor growth and metastasis by novel Carbonic Anhydrase IX Inhibitors, Cancer Res. 71 (2011) 3364–3376.
[30] A Study of SLC-0111 and Gemcitabine for Metastatic Pancreatic Ductal Cancer in Subjects Positive for CAIX-Full Text View - ClinicalTrials.gov https://clinicaltrials.gov/ct2/show/NCT03450018 (accessed Jan 24, 2019).
[31] A.D. Fiore, A. Vergara, M. Caterino, V. Alterio, S.M. Monti, J. Ombouma, P. Dumy, D. Vullo, C.T. Supuran, J.-Y. Winum, et al., Hydroxylamine-O-sulfonamide is a versatile lead compound for the development of Carbonic Anhydrase Inhibitors, Chem. Commun. 51 (2015) 11519–11522.
[32] A.G. Marshall, C.L. Hendrickson, High-resolution mass spectrometers, Annu. Rev. Anal. Chem. 1 (2008) 579–599.
[33] M. Bozdag, F. Carta, A. Angeli, S.M. Osman, F.A.S. Alasmary, Z. AlOthman, C.T. Supuran, Synthesis of N'-phenyl-N-hydroxyureas and investigation of their inhibitory activities on human Carbonic Anhydrases, Bioorg. Chem. 78 (2018) 1–6.
[34] R.G. Khalifah, The carbon dioxide hydration activity of Carbonic Anhydrase. I. Stop-flow kinetic studies on the native human isoenzymes B and C, J. Biol. Chem. 246 (1971) 2561–2573.
[35] G. Cavaletti, G. Tredici, M.G. Petruccioli, E. Dondè, P. Tredici, P. Marmiroli, C. Minoia, A. Ronchi, M. Bayssas, G. Griffon Etienne, Effects of different schedules of oxaliplatin treatment on the peripheral nervous system of the rat, Eur. J. Cancer 37 (2001) 2457–2463.
[36] L. Di Cesare Mannelli, A. Pacini, C. Matera, M. Zanardelli, T. Mello, M. De Amici, C. Dallanoce, C. Ghelardini, Involvement of A7 NAChR subtype in rat oxaliplatin-induced neuropathy: effects of selective activation, Neuropharmacology 79 (2014) 37–48.
[37] L. Di Cesare Mannelli, M. Marcoli, L. Micheli, M. Zanardelli, G. Maura, C. Ghelardini, C. Cervetto, Oxaliplatin evokes P2X7-dependent glutamate release in the cerebral cortex: a pain mechanismmediated by Pannexin 1, Neuropharmacology 97 (2015) 133–141.
[38] S. Bua, L. Di Cesare Mannelli, D. Vullo, C. Ghelardini, G. Bartolucci, A. Scozzafava, C.T. Supuran, F. Carta, Design and synthesis of novel nonsteroidal anti-inflammatory drugs and Carbonic Anhydrase Inhibitors hybrids (NSAIDs-CAIs) for the treatment of rheumatoid arthritis, J. Med. Chem. 60 (2017) 1159–1170.
[39] F. Carta, D. Vullo, A. Maresca, A. Scozzafava, C.T. Supuran, New chemotypes acting as isozyme-selective Carbonic Anhydrase Inhibitors with low affinity for the off-target cytosolic isoform II, Bioorg. Med. Chem. Lett. 22 (2012) 2182–2185.
[40] H.M. Berman, J. Westbrook, Z. Feng, G. Gilliland, T.N. Bhat, H. Weissig, I.N. Shindyalov, P.E. Bourne, The protein data bank, Nucleic Acids Res. 28 (2000) 235–242.
[41] G.M. Morris, H. Ruth, W. Lindstrom, M.F. Sanner, R.K. Belew, D.S. Goodsell, A.J. Olson, AutoDock4 and AutoDockTools4: automated docking with selective receptor flexibility, J. Comput. Chem. 30 (2009) 2785–2791.
[42] D. Santos-Martins, S. Forli, M.J. Ramos, A.J. Olson, AutoDock4Zn: an improved autodock force field for small-molecule docking to zinc metalloproteins, J. Chem. Inf. Model. 54 (2014) 2371–2379.
[43] M. Krasavin, A. Shetnev, T. Sharonova, S. Baykov, S. Kalinin, A. Nocentini, V. Sharoyko, G. Poli, T. Tuccinardi, S. Presnukhina, T.B. Tennikova, C.T. Supuran, Continued exploration of 1,2,4-oxadiazole periphery for Carbonic Anhydrase-targeting primary arene sulfonamides: discovery of subnanomolar inhibitors of membrane-bound HCA IX isoform that selectively kill cancer cells in hypoxic environment, Eur. J. Med. Chem. 164 (2019) 92–105.
[44] F. Dal Piaz, M.B. Vera Saltos, S. Franceschelli, G. Forte, S. Marzocco, T. Tuccinardi, G. Poli, S. Nejad Ebrahimi, M. Hamburger, N. De Tommasi, A. Braca, Drug affinity responsive target stability (DARTS) identifies laurifolioside as a new clathrin heavy chain modulator, J. Nat. Prod. 79 (2016) 2681–2692.
[45] M. De Leo, C.G. Huallpa, B. Alvarado, C. Granchi, G. Poli, N. De Tommasi, A. Braca, New diterpenes from salvia pseudorosmarinus and their activity as inhibitors of monoacylglycerol lipase (MAGL), Fitoterapia 130 (2018) 251–258.
[46] D.A. Case, J.T. Berryman, R.M. Betz, D.S. Cerutti, Darden, R.E. Duke, T.J. Giese, H. Gohlke, A.W. Goetz, N. Homeyer, S. Izadi, P. Janowski, J. Kaus, A. Kovalenko, T.S. Lee, S. LeGrand, P. Li, T. Luchko, R. Luo, B. Madej, K.M. Merz, G. Monard, P. Needham, H. Nguyen, H.T. Nguyen, I. Omelyan, A. Onufriev, D.R. Roe, A. Roitberg, R. Salomon-Ferrer, C.L. Simmerling, W. Smith, J. Swails, R.C. Walker, J. Wang, R. M. Wolf, X. Wu, D.M. York, P.A. Kollman, AMBER, Version 16, University of California, San Francisco, CA, 2016.
[47] L.R. Chiarelli, M. Mori, D. Barlocco, G. Beretta, A. Gelain, E. Pini, M. Porcino, G. Mori, G. Stelitano, L. Costantino, M. Lapillo, D. Bonanni, G. Poli, T. Tuccinardi, S. Villa, F. Meneghetti, Discovery and development of novel salicylate synthase (MbtI) furanic inhibitors as antitubercular agents, Eur. J. Med. Chem. 155 (2018) 754–763.
[48] J.C. McGrath, E. Lilley, Implementing guidelines on reporting research using animals (ARRIVE Etc.): new requirements for publication in BJP, Br. J. Pharmacol. 172 (2015) 3189–3193.
[49] L. Di Cesare Mannelli, A. Pacini, L. Bonaccini, M. Zanardelli, T. Mello, C. Ghelardini, Morphologic features and glial activation in rat oxaliplatin-dependent neuropathic pain, J. Pain 14 (2013) 1585–1600.
[50] L. Di Cesare Mannelli, D. Bani, A. Bencini, M.L. Brandi, L. Calosi, M. Cantore, A.M. Carossino, C. Ghelardini, B. Valtancoli, P. Failli, Therapeutic effects of the superoxide dismutase mimetic compound MnIIMe2DO2A on experimental articular pain in rats, Mediat. Inflamm. 2013 (2013) 905360.
[51] P. Failli, D. Bani, A. Bencini, M. Cantore, L. Di Cesare Mannelli, C. Ghelardini, C. Giorgi, M. Innocenti, F. Rugi, A. Spepi, R. Udisti, B. Valtancoli, A novel manganese complex effective as superoxide anion scavenger and therapeutic agent against cell and tissue oxidative injury, J. Med. Chem. 52 (2009) 7273–7283.